NANO LETTERS

pubs.acs.org/NanoLett
Letter

Discovery of Graphene Growth Alloy Catalysts Using High-Throughput Machine Learning

Xinyu Li, Javen Qinfeng Shi, and Alister J. Page*

Cite This: *Nano Lett.* 2023, 23, 9796−9802

ABSTRACT: Despite today's commercial-scale graphene production using chemical vapor deposition (CVD), the growth of high-quality single-layer graphene with controlled morphology and crystallinity remains challenging. Considerable effort is still spent on designing improved CVD catalysts for producing high-quality graphene. Conventionally, however, catalyst design has been pursued using empirical intuition or trial-and-error approaches. Here, we combine high-throughput density functional theory and machine learning to identify new prospective transition metal alloy catalysts that exhibit performance comparable to that of established graphene catalysts, such as Ni(111) and Cu(111). The alloys identified through this process generally consist of combinations of early- and late-transition metals, and a majority are alloys of Ni or Cu. Nevertheless, in many cases, these conventional catalyst metals are combined with unconventional partners, such as Zr, Hf, and Nb. The approach presented here therefore highlights an important new approach for identifying novel catalyst materials for the CVD growth of low-dimensional nanomaterials.

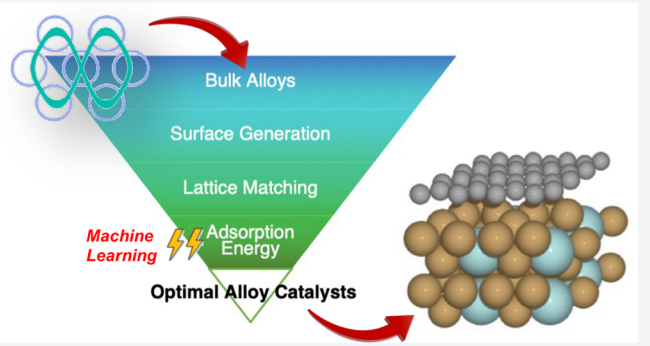

KEYWORDS: *graphene, catalyst, alloy, chemical vapor deposition, machine learning*

Over the past several decades, there has been significant interest in graphene due to its exceptional electronic, mechanical, and thermal properties,[1,2] as well as its diverse range of emerging applications. Today, chemical vapor deposition (CVD) is the principal method for producing single-layer graphene. In this process, carbon source feedstock (mostly methane, but acetylene,[3] ethanol,[4] and benzene[5−7] have also been used) is decomposed on a catalyst, typically a transition metal, at a high temperature. Despite the now-commercial scale of CVD graphene production, this technique still faces challenges, such as control over the morphology and crystallinity of single-layer graphene, control over the multilayer graphene thickness and stacking ("twist") angle, and the optimization of low-temperature conditions and semiconducting growth catalysts. These challenges mean there is still considerable focus on the improvement of CVD catalyst materials, as recently reviewed by Liu et al.[8]

This so-called "catalyst design" has led to the investigation of a wide range of catalysts that support graphene growth, including metals (e.g., Cu,[9,10] Ni,[10] and Co[11]), metalloids,[12] alloys (e.g., CuNi,[13,14] AuNi,[15] and NiMo[16]), doped metals,[17] and silicides (e.g., SiC,[18] SiN,[19] NiC,[20] and GeSi[21]). However, as with material discovery more generally, the traditional design of new CVD graphene growth catalysts has proceeded largely via empirical intuition or trial and error. For instance, CuNi alloy catalysts were gradually optimized via systematically altering the Cu:Ni alloy ratio and assessing the resultant impact on graphene morphology and quality.[13,22−24] Such endeavors have been assisted by mechanistic insights gained from theoretical studies.[17,20,25,26] The influence of fragment structure,[27,28] methane decomposition,[29] and catalyst phase,[30] for example, has been established using density functional theory (DFT). Notably, on typical graphene growth catalysts such as Ni(111) and Cu(111), these studies indicate that the critical fragment size whereupon sp^2 carbon fragments first form is approximately C_{10}−C_{12}, depending on the catalyst used. Similarly, Mitchell and Page[26] used DFT to investigate the influence of hydrogen present during graphene nucleation, concluding that hydrogen stabilizes smaller ring structures.[26]

While computational approaches can deliver important mechanistic insights regarding graphene growth, computational design of altogether-new CVD graphene growth catalysts remains impractical due to the size of the graphene growth "parameter space"[20] and the computational cost of DFT itself. In recent years, machine learning (ML) and data-driven methods have emerged as a new "fourth paradigm" for

Received: July 5, 2023
Revised: October 5, 2023
Published: October 27, 2023

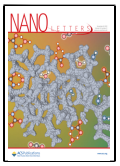

https://doi.org/10.1021/acs.nanolett.3c02496
Nano Lett. 2023, 23, 9796−9802

scientific research and exploration.[31] Such approaches have achieved notable recent success regarding the prediction of the molecular, crystalline, and catalytic properties in particular[32−34] and have led to the development of new catalysts for fundamental reactions such as hydrogen evolution,[35] CO_2 reforming,[36] and biomass reforming.[37] Despite these successes, the use of high-throughput and machine learning approaches for studying the chemical reactions and systems relevant to nanoscale self-assembly processes, such as graphene growth, remains largely unexplored. Presumably, this is a result of their inherent data dependency and the cost associated with generating sufficiently large training sets using DFT (a cost that is less onerous when studying smaller molecular systems). One notable exception is the ARES (autonomous research system) approach pioneered by Maruyama et al.,[38] which is capable of guiding high-throughput experimental studies of single-walled carbon nanotube growth.[39]

Herein, we report a machine learning-aided high-throughput approach (Figure 1) for the discovery of new binary transition metal alloys (TMAs) for CVD graphene growth. Initially, 1499 suitable transition and post-transition metal alloys available in Materials Project[40] were used to generate 12 671 low-index candidate catalyst surfaces. These initial surfaces were then screened using geometrical constraints and used to construct data sets of carbon and benzene adsorption complexes to train machine learning models. The final recommendation for prospective alloy catalysts is based on multiple catalytic descriptors, including the adsorption energies of relevant carbonaceous precursor species and graphene itself. To circumvent the DFT efficiency bottleneck here, adsorption energies of carbon and benzene were first predicted using machine learning (ML), with DFT being used to verify only a handful of optimal catalysts. Ultimately, we propose 10 new prospective alloy surfaces that, to the best of our knowledge, have never been considered as CVD graphene growth catalysts. The carbon and benzene adsorption energy data sets cover a wide range of catalyst materials without geometric constraints, which provide a useful foundation for expediting the discovery of catalysts for various carbon material growth applications.

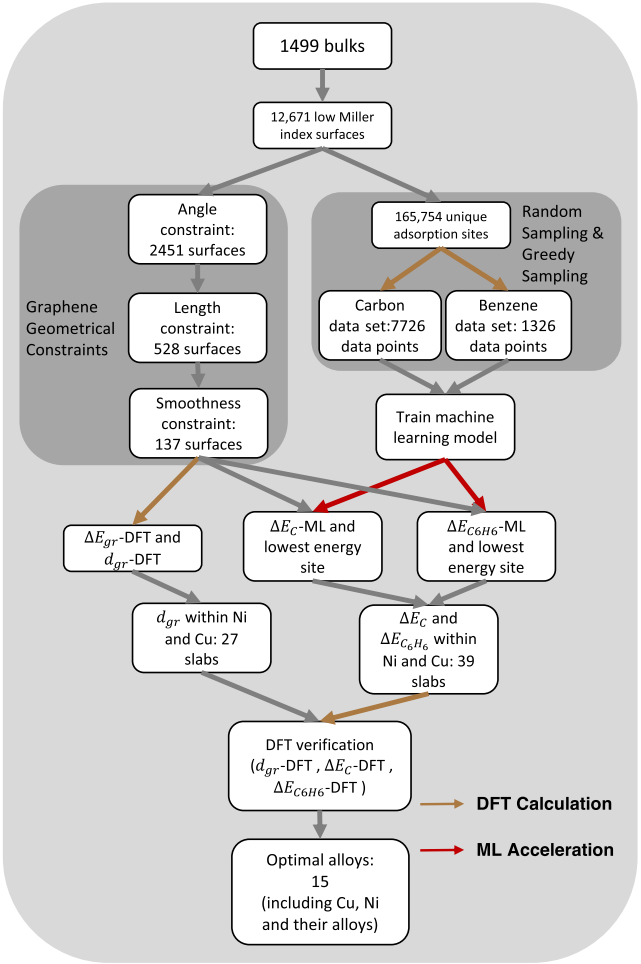

Figure 1. High-throughput framework used to discover new alloy catalysts for graphene growth.

We begin our discussion by detailing the search space for discovering new alloy catalysts. TMAs have emerged as a potential solution for overcoming the limitations of pure metal graphene growth catalysts such as the low catalytic activity of Cu and the high carbon solubility of Ni. Notable examples include NiCu,[13,14] AuNi,[15] and NiMo.[16] However, a vast number of transition metal alloys remain unexplored due to their extensive design space and the low efficiency of conventional experimental and computational methods. Therefore, our search space includes all transition metals except for Tc (as it is rare and radioactive) and Hg (as it has a low melting point), see Figure S1. Four post-transition metals with melting points of >573 K (Al, Zn, Tl, and Cd) are included because graphene growth on post-transition metal catalysts remains relatively unexplored. Moreover, post-transition metals typically exhibit a weak adsorption energy, which is favorable for graphene growth. The primary concern with post-transition metals lies in their instability under oxygen conditions. Nevertheless, creating a reducing environment for graphene growth is feasible. We limit this study to metal alloys only and do not consider metal carbide, oxide, or silicide phases. Bulk alloy structures were extracted from both Materials Project[40] and the data set of Mamun et al.[34] The latter includes $L1_0$ and $L1_2$ type alloys that potentially possess crystal lattice dimensions commensurate to those of graphene but are absent from Materials Project. To restrict our search space to stable materials, only bulk crystals with negative formation energies and ΔE_{hull} values of ≤0.2 eV/atom were included. Ultimately, this restriction led to a search space consisting of 1499 prospective alloys, and 12 671 low-Miller index surfaces were constructed for these alloys.

An optimal CVD graphene growth catalyst should have a degree of structural epitaxy with the growing graphene structure.[41] While perfect epitaxy can lead to difficulty in postgrowth separation due to overly strong adsorption, large degrees of lattice mismatch between graphene and the growth catalyst yield even greater challenges for producing high-quality single-layer graphene during CVD. Therefore, we applied three geometrical criteria to narrow down the number of candidate catalysts: the degree of epitaxy (angle), the lattice vector match (length), and surface smoothness. The first geometric criterion, the degree of epitaxy between the graphene primitive lattice and each metal surface, is shown in Figure 2a. Specifically, we have restricted our search space to metal surfaces with lattice angles γ such that $\mathrm{mod}(\gamma, 60) \leq \pm 1°$ [or $\mathrm{mod}(\gamma, 120) \leq \pm 1°$]. For surfaces within the search space with reduced cells corresponding to $\gamma \approx 90°$, six additional catalyst superlattices were also generated, as shown in Figure 2b. Ultimately, these criteria yielded 2451 catalyst surfaces. Of

https://doi.org/10.1021/acs.nanolett.3c02496
Nano Lett. 2023, 23, 9796−9802

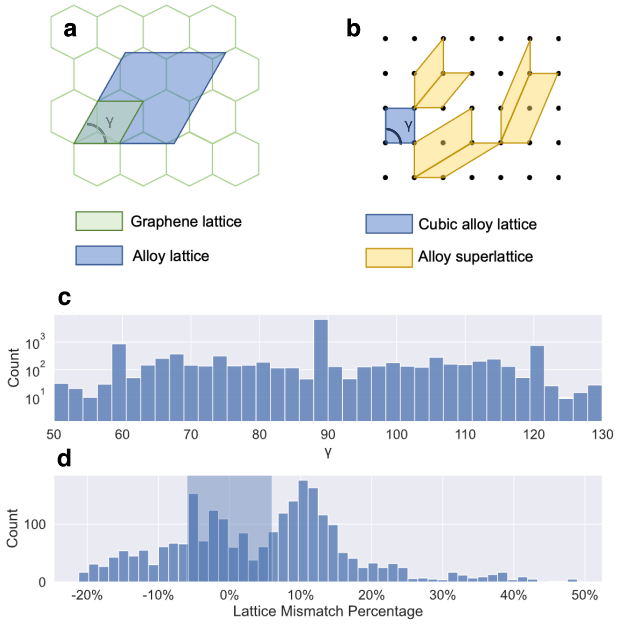

Figure 2. (a) Alloy lattices are commensurate with the adsorbed graphene lattice when the metal lattice has $\gamma \approx 60°$. For cubic lattices ($\gamma \approx 90°$), six additional alloy superlattices were generated, shown in panel b, to ensure compatible alloy surfaces were included in the search space. (c) γ values (degrees) and (d) degrees of lattice mismatch in length (with respect to graphene, percent) for the 1499 bulk alloy lattices; 2451 low-index alloy surfaces have $\gamma = 60 \pm 1°$, and 137 surfaces have lattice vectors within 6% of the graphene value of 2.46 Å.

these, only 528 surfaces possess lattice vectors within 6% of the graphene lattice vector (2.46 Å). We note that this tolerance exceeds the mismatch of established graphene growth catalysts [e.g., Cu(111), ∼4.07%; Ni(111), ∼1.22%[42]] so that prospective catalysts are not inadvertently excluded. Finally, by restricting our search space to those flat and smooth surfaces [e.g., the close-packed (111) surface for fcc crystals], we are left with 137 prospective alloy catalyst surfaces, as summarized in Table S1, which yield 1333 (carbon) and 2666 (benzene) distinct adsorption sites. Machine learning is then employed to accelerate the calculation of these adsorption energies, with full DFT calculations used for only the most stable sites for each catalyst. The best 10 catalysts found using this algorithm are detailed in Table 1. Table 1 also lists the descriptors of established graphene growth catalysts [(111) facets of Cu, Ni, Cu_3Ni, Ni_2Cu_2, and Ni_3Cu] for comparison. Full details of all prospective catalysts are provided in the Supporting Information. Figure 1 provides full details of the screening algorithm employed here.

Theoretical studies of CVD catalysts commonly assess catalyst performance via their affinity for graphene itself, for instance, in terms of graphene's adsorption energy. Nevertheless, the optimal graphene adsorption energy is a necessary but not sufficient condition for a substrate to be an effective graphene growth catalyst. Hydrocarbon activation and carbon dissolution are both critical processes during graphene growth and can be described by carbon adsorption energies according to the descriptor-based microkinetic modeling[43] and Brønsted−Evans−Polanyi relations.[44] It also has been shown that carbon atoms are more dominant than other carbon radicals (CH_i, where i = 1, 2, 3, or 4) on Cu(111), Ni(111), Ir(111), and Rh(111) surfaces[29] and drive the formation and growth of sp carbon chains that ultimately oligomerize and aggregate into sp^2 "islands" and subsequently larger graphene structures.[45] The latter can be adsorbed directly on the catalyst surface or reside within it via a "sunken" growth mode.[46]

We therefore sought to assess the utility of the prospective 137 alloy catalysts with respect to each individual step of this mechanism. That is, we consider the adsorption energy of graphene itself, as well as those of activated carbon atoms and fragments on the catalyst surface for each of these alloys (here, our proxy for small sp^2 islands is benzene, which is an established precursor for CVD graphene growth itself[5−7]). We consider in greater detail the reliability of using adsorption energies of individual species for predicting catalyst performance in the Supporting Information and demonstrate that

Table 1. Compositions, Materials Project IDs, Miller Indices, Terminations, Graphene Adsorption Energies (ΔE_{gr}, electronvolts per C atom), Graphene Adsorption Distances (d_{gr}, angstroms), Carbon Adsorption Energies (ΔE_C, electronvolts), and Benzene Adsorption Energies ($\Delta E_{C_6H_6}$, electronvolts) of Optimal Prospective Alloys for Graphene Growth[a]

alloy	Materials Project ID	facet	termination	% mismatch	ΔE_{gr}	d_{gr}	$\Delta E_{C_6H_6}$	ΔE_C
$ZrPd_2$	mp-1018102	110	Pd−Zr	0.77	−0.10	2.24	−1.52	0.13
YCu_5	mp-2797	001	Y−Cu	1.04	−0.05	3.04	−1.26	0.13
$ZnNi_3$	mp-971758	111	Ni−Zn	1.07	−0.06	2.19	−1.21	−1.16
Sc_2Ni_4	mp-850	111	Ni	−2.02	−0.07	2.19	−1.47	−0.61
Hf_2Ni_4	mp-30708	111	Ni	−2.28	−0.07	2.34	−1.76	−0.37
$ZrCu_5$	mp-30603	111	Cu	−2.44	−0.06	3.12	−1.01	0.57
$ZrCu_5$	mp-30603	111	Zr−Cu	−2.44	−0.05	3.10	−1.33	0.21
Ni_3Pt	mp-12798	111	Ni−Pt	3.14	−0.07	2.20	−2.03	−0.76
Nb_2Ni_4	mp-1077429	111	Nb−Ni	−3.26	−0.07	2.35	−1.73	−0.76
$MoPd_2$	mp-1206704	110	Pd−Mo	−3.66	−0.06	3.26	−1.21	−0.20
Ni_3Cu	cif-Ni3Cu	111	Cu−Ni	0.08	−0.05	2.22	−1.97	−0.99
Ni_2Cu_2	cif-NiCu	101	Cu−Ni	−0.93	−0.04	2.22	−1.65	−0.50
Cu_3Ni	cif-Cu3Ni	111	Cu−Ni	1.46	−0.07	3.28	−1.32	0.29
Cu	mp-30	111	Cu	2.32	−0.06	3.28	−1.08	1.15
Ni	mp-23	111	Ni	−0.53	−0.07	2.19	−2.28	−0.94

[a]Carbon and benzene adsorption energies were calculated by using RPBE-D3, while graphene was calculated by using SCAN-rVV10. Values for Cu_3Ni(111), Ni_2Cu_2(101), and Ni_3Cu(111) alloys and Cu(111) and Ni(111) are included for comparison.

https://doi.org/10.1021/acs.nanolett.3c02496
Nano Lett. 2023, 23, 9796−9802

better performance is obtained when they are considered collectively. Note that here we have not investigated subsurface dissolution, as it has shown that the production of single-layer graphene on Cu(111) and Ni(111) is driven by a surface-mediated mechanism.[29] Ultimately, the recommendations made below are based upon consideration of these adsorption energies (or adsorption distance) and the physical structure of the catalyst itself and are most relevant to surface-mediated growth of single-layer graphene. We note that the use of machine learning here to predict distinct carbon and benzene adsorption energies effectively enables the use of multiple descriptors for each prospective catalyst; this would otherwise not be practical due to the number of DFT adsorption energy calculations involved with the data sets employed here.

Panels a and b of Figure 3 validate ML-predicted carbon and benzene adsorption energies, respectively, against DFT values

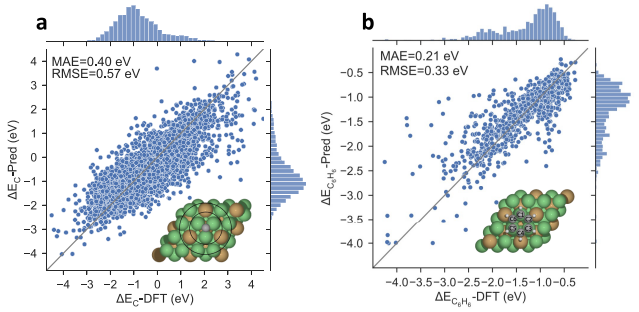

Figure 3. (a) Comparison of ML-predicted carbon adsorption energies (ΔE_C, electronvolts) and DFT values for 7726 adsorption complexes (5269 alloy surfaces). (b) Comparison of ML-predicted benzene adsorption energies ($\Delta E_{C_6H_6}$, electronvolts) and DFT values for 1326 adsorption complexes (206 alloy surfaces). The insets show the adsorption structures of C and C_6H_6 on a binary transition metal (111) surface facet.

using the generated data sets, which are later used as the training set to predict optimal catalysts. Illustrative examples of carbon, benzene, and graphene adsorption complexes are provided in Figure 5. Note that we expect the carbon and benzene data set generated in this study can be used for other carbon materials in the future, so the catalyst surfaces are not

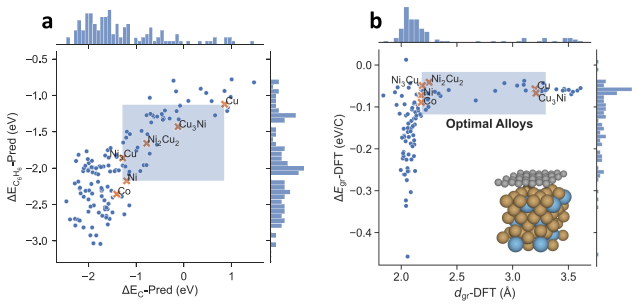

Figure 4. (a) ML-predicted benzene adsorption energies vs ML-predicted carbon adsorption energies. (b) Comparison of DFT adsorption energies of graphene (electronvolts per C atom) and adsorption distances (angstroms) on 137 prospective alloy catalyst surfaces. The blue highlighted region indicates optimal catalysts; established Co, Ni, and Cu pure metals and NiCu alloys are highlighted. The insets show the adsorption structures of graphene on a binary transition metal (111) surface facet.

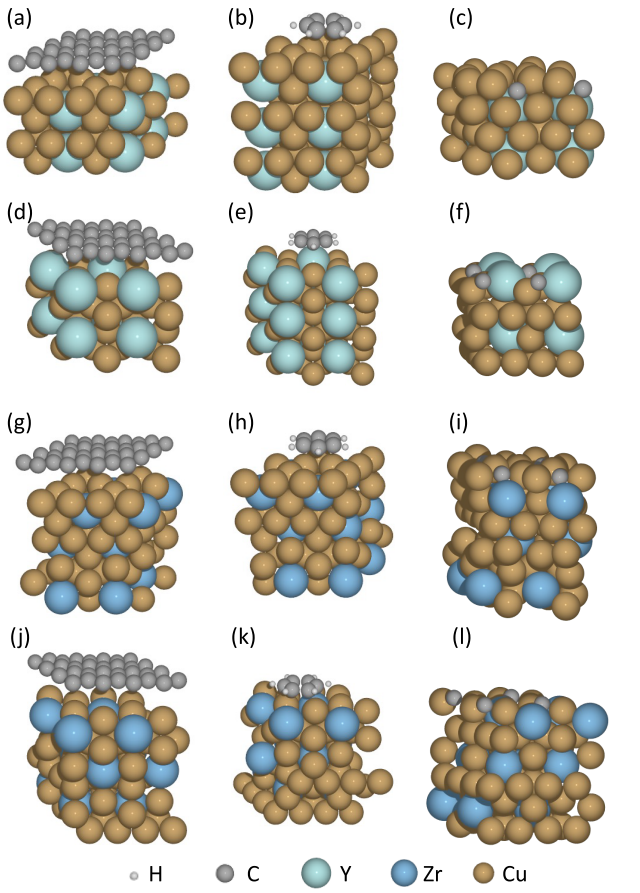

Figure 5. Adsorption of graphene, benzene, and carbon on (a–c) the YCu_5 Cu-terminated surface, (d–f) the YCu_5 Y–Cu-terminated surface, (g–i) the $ZrCu_5$ Cu-terminated surface, and (j–l) the $ZrCu_5$ Zr–Cu-terminated surface.

limited to the 137 geometry-filtered surfaces (see Methods for details on this data set). For carbon and benzene adsorption (Figure 3a,b), the comparison is based on individual adsorption complexes; Figure 3 shows that the ML algorithm GemNet-OC performs comparably in describing both carbon and benzene adsorption. For graphene adsorption, we find that utilizing GemNet-OC for prediction is appropriate, as indicated in Figure S7. However, we refrained from using the machine learning-predicted graphene adsorption energy in our investigation because it is practical to use DFT to calculate graphene adsorption energies on all 137 catalysts directly. All graphene adsorption-related values in the remainder of our discussion are DFT values. Figure 4a compares the ML-predicted carbon and benzene adsorption energies for the most favorable adsorption sites on the 137 surfaces listed in Table S1. A validation of these predicted values is shown in Figure S2, which shows that the ML-predicted and DFT-calculated adsorption energies are well correlated. Li et al.[37] showed that, to predict accurate adsorption energies on a given metal, the training set needs to include only a relatively small number of adsorption energies (e.g., 20%) on that metal, provided that it includes a sufficiently diverse range of metal surfaces. Thus, while the training set here is only approximately twice that of the test set, the reliability of our ML-predicted adsorption energies is ensured by the use of a greedy sampling approach, which guarantees inclusion of at least one sample from each alloy surface. Figure 4a compares ML-predicted carbon and

https://doi.org/10.1021/acs.nanolett.3c02496
Nano Lett. 2023, 23, 9796–9802

benzene adsorption energies on the 137 catalysts considered here and shows a good correlation, as anticipated. For these alloy surfaces, there is no example of a catalyst that binds carbon weakly, while binding benzene strongly. On the contrary, there are a small number of catalysts that yield the opposite behavior. Figure S3 shows (for Zr_4Ru_8 as an example) that this is a product of surface termination, enabling intercalation, or subsurface adsorption, of carbon atoms. Having validated the ML approach using carbon and benzene adsorption energies, we now consider which of the 137 catalysts are potential graphene growth catalysts. The adsorption behavior of the best-performing non-alloy graphene catalysts, Ni(111) and Cu(111), defines the range of what we consider "optimal" performance here. We gauge this behavior via the adsorption energies of carbon (ΔE_C-ML), benzene ($\Delta E_{C_6H_6}$-ML), and graphene (ΔE_{gr}-DFT), as well as the graphene−metal adsorption distance (d_{gr}-DFT). These ranges are highlighted in blue in panels a and b of Figure 4 (they are also highlighted in Table S1). Graphene adsorption energies on established growth catalysts, i.e., pristine Cu(111), Ni(111), and Co(0001) facets, and (111) facets of Cu_3Ni, Ni_2Cu_2, and Ni_3Cu alloys are also highlighted in panels a and b of Figure 4 as points of reference. We note that NiCu alloy catalysts, established for graphene growth, fall within the highlighted range in panels a and b of Figure 4, which provides confidence in our approach.

Figure 4b shows that ΔE_{gr}-DFT and d_{gr}-DFT values for the 137 alloys considered here are grouped into two clusters. The first comprises alloys yielding adsorption distances of 1.84−2.42 Å, indicating a strong interaction with graphene, akin to that observed for Co(0001) and Ni(111) metal catalysts (2.15 and 2.19 Å, respectively). The second consists of alloys that adsorb graphene at longer distances of 3.04−3.60 Å, indicating weaker interaction with graphene, akin to that observed for Cu(111) and Cu_3Ni (3.28 Å for both of them). Of these 137 alloys, 27 fall within the ΔE_{gr}-DFT and d_{gr}-DFT values of Cu(111) and Ni(111) (see Table S1). Other prospective catalysts for graphene growth include various combinations of early- and late-transition metals. The top 10 are listed in Table 1; to the best of our knowledge, none of these alloys have been investigated as graphene growth catalysts. We note that while our threshold for graphene epitaxy is relatively loose (6%), the prospective alloy catalysts listed in Table 1 have lattice mismatches that fall well below this threshold (≤3.6%).

The prospective alloy catalysts identified in Table 1 indicate that combining early- and late-transition metals yields high-performing CVD graphene growth catalysts; this motif is featured in eight of the ten catalysts discovered here. Considering established descriptors for predicting heterogeneous catalysis such as d-band theory,[47] this is perhaps unsurprising, because the superposition of higher- and lower-energy d-band energies (provided by the early- and late-transition metal, respectively) affords a mix of states that can interact optimally with adsorbing carbonaceous species and graphene itself.[48] Nevertheless, to the best of our knowledge, this strategy has not been pursued widely in the CVD growth of nanocarbon structures such as graphene and CNTs. Exceptions to this alloy motif are $ZnNi_3$ and Ni_3Pt. Table 1 shows that the performance of the Ni−Zn-terminated (111) surface of this alloy is comparable to that of NiCu alloys, at least according to the four descriptors employed here. This performance can be rationalized by the fact that Zn is a d^{10} post-transition metal with a generally weak adsorption strength,[49] so Zn here may in fact be mimicking the role played by Cu in Ni−Cu alloy catalysts. The catalytic descriptors for Ni_3Pt indicate its potential as an alloy with its catalytic activity falling between those of Ni and Ni_3Cu, but with a larger mismatch (3.14%).

Another persistent feature in the alloys identified in Table 1 is the inclusion of Ni and Cu; all but three of the catalysts discovered here incorporate Ni or Cu to some degree. Considering the performance of Cu(111), Ni(111), and Ni−Cu alloys for CVD graphene growth, this is anticipated. Of these six Ni/Cu alloys, d^0 (Y and Sc) and d^1 (Zr and Hf) metals feature in the majority, again highlighting the early/late-transition metal motif mentioned above. Ni here is more versatile than Cu in this respect. Of the seven Ni/Cu alloys, five are Ni-based ($ZnNi_3$, Sc_2Ni_4, Hf_2Ni_4, Ni_3Pt, and Nb_2Ni_4) while only two are Cu-based (YCu_5 and $ZrCu_5$, noting however the latter affords two distinct surface terminations that exhibit similar performance). We computed the density of states (DOS) for YCu_5 and $ZrCu_5$, and the results are depicted in Figure S11. The two Cu-terminated surfaces exhibit an electronic structure akin to that of Cu(111). However, in the case of Y−Cu- and Zr−Cu-terminated surfaces, there is evidence of an increased DOS above the Fermi energy. This similarity to Cu−Ni alloys is consistent with their comparable catalytic performance (according to the adsorption energy descriptors employed here). The two alloys that exclude Ni and Cu, i.e., $ZrPd_2$ and $MoPd_2$, are alloys of Pd, which is a metal also established as a graphene growth catalyst. In each case, these alloys share a similar surface termination that comprises both metals in the alloy. Nb is also found in the alloy Nb_2Ni_4, which exhibits adsorption energy descriptors comparable to those of the Ni−Cu catalysts listed in Table 1, albeit with a significantly larger lattice mismatch (−3.26%).

We believe all alloys listed in Table 1 should be compatible with typical graphene growth conditions, and all exhibit stable phases at typical CVD temperatures.[50] For instance, compared to the melting point of bulk Ni (1455 °C), the Ni alloys in Table 1 have generally marginally lower melting points (Nb_2Ni_4, ∼1340 °C; Hf_2Ni_4, ∼1280 °C; Sc_2Ni_4, ∼1340 °C). $ZnNi_3$ is an outlier, which melts at ∼780 °C. The two Cu alloys listed in Table 1 have phase stability comparable to that of Cu itself (e.g., $ZrCu_5$ melts at ∼1100 °C, and YCu_5 at ∼950 °C[51]). Unsurprisingly, the Pd and Pt alloys in Table 1 have high melting points ($MoPd_2$, ∼1720 °C; $ZrPd_2$, ∼1600 °C;[52] Ni_3Pt, ∼1510 °C[50]).

In conclusion, we have identified new prospective transition metal alloy catalysts for graphene CVD growth via a high-throughput machine learning approach. By screening 12 671 catalyst surfaces on purely geometrical considerations, we revealed 137 surfaces with lattice structures commensurate with graphene. By combining machine learning prediction and DFT calculation, we obtained carbon, benzene, and graphene adsorption simultaneously on these alloy surfaces. This led to 10 new prospective alloy catalysts that exhibit performance comparable to those of established graphene catalysts, such as Ni(111) and Cu(111). Despite the relatively "mindless" approach taken here, the alloys that were identified here have somewhat unsurprising characteristics. For example, all except one are combinations of early- and late-transition metals, as is the case for many high-performance heterogeneous catalysts. Similarly, a majority are alloys of Ni or Cu (with the remainder being alloys of Pd, which is also capable of

https://doi.org/10.1021/acs.nanolett.3c02496
Nano Lett. 2023, 23, 9796−9802

supporting the CVD growth of graphene). Nevertheless, in many cases, these conventional metals are alloyed with unexpected partners, for instance, Zr, Hf, and Nb. We believe that these alloys have not previously been considered as graphene growth catalysts. This investigation therefore highlights an important, yet underutilized, approach for novel CVD catalyst discovery and catalyst optimization for graphene and low-dimensional nanomaterial growth more generally. In addition, the ML data set constructed here to predict the adsorption energies of carbon-related species will be a useful resource for gaining deeper insights into two-dimensional material growth, for instance, by expediting development of microkinetic models of hydrocarbon decomposition on alloy catalysts. It could also serve future heterogeneous catalysis research more widely, by leveraging its ∼9000 structures with techniques like transfer learning[53] and self-supervised learning.[54]

■ ASSOCIATED CONTENT

Supporting Information

The Supporting Information is available free of charge at https://pubs.acs.org/doi/10.1021/acs.nanolett.3c02496.

Full computational method details; detailed adsorption energy descriptors on the 137 flat and smooth slabs; performance of single adsorption energy descriptors versus collective adsorption energy descriptors; ML prediction verification; details of the group and period-based coordination fingerprint for carbon and its improved version for benzene; comparison of ML algorithms; and illustrative examples of strong carbon but weak benzene adsorption surfaces, unique adsorption sites, and benzene rotation (PDF)

■ AUTHOR INFORMATION

Corresponding Author

Alister J. Page − *Discipline of Chemistry, School of Environmental and Life Sciences, The University of Newcastle, Callaghan, New South Wales 2308, Australia;* orcid.org/0000-0002-8444-2775; Email: alister.page@newcastle.edu.au

Authors

Xinyu Li − *School of Information and Physical Sciences, The University of Newcastle, Callaghan, New South Wales 2308, Australia; Australian Institute for Machine Learning, The University of Adelaide, Adelaide, South Australia 5000, Australia;* orcid.org/0000-0003-1332-9203

Javen Qinfeng Shi − *Australian Institute for Machine Learning, The University of Adelaide, Adelaide, South Australia 5000, Australia*

Complete contact information is available at: https://pubs.acs.org/10.1021/acs.nanolett.3c02496

Notes

The authors declare no competing financial interest.

■ ACKNOWLEDGMENTS

X.L. acknowledges a Higher Degree by Research (HDR) scholarship from The University of Newcastle, Australia, and financial support from the Center for Augmented Reasoning, Australian Institute for Machine Learning. This research was funded by the Australian Government through the Australian Research Council (DP210100873). This research was undertaken with the assistance of resources provided at the NCI National Facility Systems at the Australian National University and INTERSECT systems, through the National Computational Merit Allocation Scheme supported by the Australian Government.

■ REFERENCES

(1) Zhang, Z.; Du, Y.; Huang, S.; Meng, F.; Chen, L.; Xie, W.; Chang, K.; Zhang, C.; Lu, Y.; Lin, C.-T.; et al. Macroscale superlubricity enabled by graphene-coated surfaces. *Adv. Sci.* **2020**, *7*, 1903239.

(2) Johari, P.; Shenoy, V. B. Modulating optical properties of graphene oxide: Role of prominent functional groups. *ACS Nano* **2011**, *5*, 7640−7647.

(3) Ramón, M. E.; Gupta, A.; Corbet, C.; Ferrer, D. A.; Movva, H. C. P.; Carpenter, G.; Colombo, L.; Bourianoff, G.; Doczy, M.; Akinwande, D.; et al. CMOS-compatible synthesis of large-area, high-mobility graphene by chemical vapor deposition of acetylene on cobalt thin films. *ACS Nano* **2011**, *5*, 7198−7204.

(4) Guermoune, A.; Chari, T.; Popescu, F.; Sabri, S. S.; Guillemette, J.; Skulason, H. S.; Szkopek, T.; Siaj, M. Chemical vapor deposition synthesis of graphene on copper with methanol, ethanol, and propanol precursors. *Carbon* **2011**, *49*, 4204−4210.

(5) Dai, G.-P.; Cooke, P. H.; Deng, S. Direct growth of graphene films on TEM nickel grids using benzene as precursor. *Chem. Phys. Lett.* **2012**, *531*, 193−196.

(6) Jang, J.; Son, M.; Chung, S.; Kim, K.; Cho, C.; Lee, B. H.; Ham, M.-H. Low-temperature-grown continuous graphene films from benzene by chemical vapor deposition at ambient pressure. *Sci. Rep.* **2015**, *5*, 17955.

(7) Khan, M. H.; Moradi, M.; Dakhchoune, M.; Rezaei, M.; Huang, S.; Zhao, J.; Agrawal, K. V. Hydrogen sieving from intrinsic defects of benzene-derived single-layer graphene. *Carbon* **2019**, *153*, 458−466.

(8) Liu, F.; Li, P.; An, H.; Peng, P.; McLean, B.; Ding, F. Achievements and challenges of graphene chemical vapor deposition growth. *Adv. Funct. Mater.* **2022**, *32*, 2203191.

(9) Li, X.; Cai, W.; An, J.; Kim, S.; Nah, J.; Yang, D.; Piner, R.; Velamakanni, A.; Jung, I.; Tutuc, E.; et al. Large-area synthesis of high-quality and uniform graphene films on copper foils. *Science* **2009**, *324*, 1312−1314.

(10) Lee, Y.; Bae, S.; Jang, H.; Jang, S.; Zhu, S.-E.; Sim, S. H.; Song, Y. I.; Hong, B. H.; Ahn, J.-H. Wafer-scale synthesis and transfer of graphene films. *Nano Lett.* **2010**, *10*, 490−493.

(11) Eom, D.; Prezzi, D.; Rim, K. T.; Zhou, H.; Lefenfeld, M.; Xiao, S.; Nuckolls, C.; Hybertsen, M. S.; Heinz, T. F.; Flynn, G. W. Structure and electronic properties of graphene nanoislands on Co(0001). *Nano Lett.* **2009**, *9*, 2844−2848.

(12) Lee, J.-H.; Lee, E. K.; Joo, W.-J.; Jang, Y.; Kim, B.-S.; Lim, J. Y.; Choi, S.-H.; Ahn, S. J.; Ahn, J. R.; Park, M.-H.; et al. Wafer-scale growth of single-crystal monolayer graphene on reusable hydrogen-terminated germanium. *Science* **2014**, *344*, 286−289.

(13) Chen, S.; Cai, W.; Piner, R. D.; Suk, J. W.; Wu, Y.; Ren, Y.; Kang, J.; Ruoff, R. S. Synthesis and characterization of large-area graphene and graphite films on commercial Cu−Ni alloy foils. *Nano Lett.* **2011**, *11*, 3519−3525.

(14) Dong, J.; Zhang, L.; Ding, F. Kinetics of graphene and 2D materials growth. *Adv. Mater.* **2019**, *31*, 1801583.

(15) Weatherup, R. S.; Dlubak, B.; Hofmann, S. Kinetic control of catalytic CVD for high-quality graphene at low temperatures. *ACS Nano* **2012**, *6*, 9996−10003.

(16) Dai, B.; Fu, L.; Zou, Z.; Wang, M.; Xu, H.; Wang, S.; Liu, Z. Rational design of a binary metal alloy for chemical vapour deposition growth of uniform single-layer graphene. *Nat. Commun.* **2011**, *2*, 522.

(17) Mitchell, I.; Irle, S.; Page, A. J. Inducing regioselective chemical reactivity in graphene with alkali metal intercalation. *Phys. Chem. Chem. Phys.* **2018**, *20*, 19987−19994.

(18) Mishra, N.; Boeckl, J.; Motta, N.; Iacopi, F. Graphene growth on silicon carbide: A review. *Phys. Status Solidi A* **2016**, *213*, 2277−2289.
(19) Chen, J.; Guo, Y.; Wen, Y.; Huang, L.; Xue, Y.; Geng, D.; Wu, B.; Luo, B.; Yu, G.; Liu, Y. Two-stage metal-catalyst-free growth of high-quality polycrystalline graphene films on silicon nitride substrates. *Adv. Mater.* **2013**, *25*, 992−997.
(20) Jiao, M.; Qian, H.; Page, A.; Li, K.; Wang, Y.; Wu, Z.; Irle, S.; Morokuma, K. Graphene nucleation from amorphous nickel carbides: QM/MD studies on the role of subsurface carbon density. *J. Phys. Chem. C* **2014**, *118*, 11078−11084.
(21) Pasternak, I.; Wesolowski, M.; Jozwik, I.; Lukosius, M.; Lupina, G.; Dabrowski, P.; Baranowski, J. M.; Strupinski, W. Graphene growth on Ge(100)/Si(100) substrates by CVD method. *Sci. Rep.* **2016**, *6*, 21773.
(22) Wu, Y.; Chou, H.; Ji, H.; Wu, Q.; Chen, S.; Jiang, W.; Hao, Y.; Kang, J.; Ren, Y.; Piner, R. D.; et al. Growth mechanism and controlled synthesis of AB-stacked bilayer graphene on Cu−Ni alloy foils. *ACS Nano* **2012**, *6*, 7731−7738.
(23) Wu, T.; Zhang, X.; Yuan, Q.; Xue, J.; Lu, G.; Liu, Z.; Wang, H.; Wang, H.; Ding, F.; Yu, Q.; et al. Fast growth of inch-sized single-crystalline graphene from a controlled single nucleus on Cu−Ni alloys. *Nat. Mater.* **2016**, *15*, 43−47.
(24) Huang, M.; Biswal, M.; Park, H. J.; Jin, S.; Qu, D.; Hong, S.; Zhu, Z.; Qiu, L.; Luo, D.; Liu, X.; et al. Highly oriented monolayer graphene grown on a Cu/Ni(111) alloy foil. *ACS Nano* **2018**, *12*, 6117−6127.
(25) Page, A. J.; Mitchell, I.; Li, H.-B.; Wang, Y.; Jiao, M.-g.; Irle, S.; Morokuma, K. Spanning the parameter space of chemical vapor deposition graphene growth with quantum chemical simulations. *J. Phys. Chem. C* **2016**, *120*, 13851−13864.
(26) Mitchell, I.; Page, A. The influence of hydrogen on transition metal - Catalysed graphene nucleation. *Carbon* **2018**, *128*, 215−223.
(27) Gao, J.; Yip, J.; Zhao, J.; Yakobson, B. I.; Ding, F. Graphene nucleation on transition metal surface: Structure transformation and role of the metal step edge. *J. Am. Chem. Soc.* **2011**, *133*, 5009−5015.
(28) Van Wesep, R. G.; Chen, H.; Zhu, W.; Zhang, Z. Communication: Stable carbon nanoarches in the initial stages of epitaxial growth of graphene on Cu(111). *J. Chem. Phys.* **2011**, *134*, 171105.
(29) Shu, H.; Tao, X.-M.; Ding, F. What are the active carbon species during graphene chemical vapor deposition growth? *Nanoscale* **2015**, *7*, 1627−1634.
(30) Li, H.-B.; Page, A. J.; Hettich, C.; Aradi, B.; Köhler, C.; Frauenheim, T.; Irle, S.; Morokuma, K. Graphene nucleation on a surface-molten copper catalyst: Quantum chemical molecular dynamics simulations. *Chem. Sci.* **2014**, *5*, 3493−3500.
(31) Schleder, G. R.; Padilha, A. C. M.; Acosta, C. M.; Costa, M.; Fazzio, A. From DFT to machine learning: recent approaches to materials science−a review. *J. Phys.: Mater.* **2019**, *2*, 032001.
(32) De Luna, P.; Wei, J.; Bengio, Y.; Aspuru-Guzik, A.; Sargent, E. Use machine learning to find energy materials. *Nature* **2017**, *552*, 23−27.
(33) Faber, F. A.; Hutchison, L.; Huang, B.; Gilmer, J.; Schoenholz, S. S.; Dahl, G. E.; Vinyals, O.; Kearnes, S.; Riley, P. F.; von Lilienfeld, O. A. Prediction errors of molecular machine learning models lower than hybrid DFT error. *J. Chem. Theory Comput.* **2017**, *13*, 5255−5264.
(34) Mamun, O.; Winther, K. T.; Boes, J. R.; Bligaard, T. High-throughput calculations of catalytic properties of bimetallic alloy surfaces. *Sci. Data* **2019**, *6*, 76.
(35) Tran, K.; Ulissi, Z. W. Active learning across intermetallics to guide discovery of electrocatalysts for CO_2 reduction and H_2 evolution. *Nat. Catal.* **2018**, *1*, 696−703.
(36) Zhong, M.; Tran, K.; Min, Y.; Wang, C.; Wang, Z.; Dinh, C.-T.; De Luna, P.; Yu, Z.; Rasouli, A. S.; Brodersen, P.; et al. Accelerated discovery of CO_2 electrocatalysts using active machine learning. *Nature* **2020**, *581*, 178−183.
(37) Li, X.; Chiong, R.; Hu, Z.; Cornforth, D.; Page, A. J. Improved representations of heterogeneous carbon reforming catalysis using machine learning. *J. Chem. Theory Comput.* **2019**, *15*, 6882−6894.
(38) Nikolaev, P.; Hooper, D.; Webber, F.; Rao, R.; Decker, K.; Krein, M.; Poleski, J.; Barto, R.; Maruyama, B. Autonomy in materials research: a case study in carbon nanotube growth. *npj Comput. Mater.* **2016**, *2*, 16031.
(39) Everhart, B. M.; Rao, R.; Nikolaev, P.; Liu, T.-W.; Gómez-Gualdrón, D. A.; Maruyama, B.; Amama, P. B. High-throughput experimentation for selective growth of small-diameter single-wall carbon nanotubes using Ru-promoted Co catalysts. *Chem. Mater.* **2022**, *34*, 4548−4559.
(40) Jain, A.; Ong, S. P.; Hautier, G.; Chen, W.; Richards, W. D.; Dacek, S.; Cholia, S.; Gunter, D.; Skinner, D.; Ceder, G.; et al. Commentary: The materials project: A materials genome approach to accelerating materials innovation. *APL Mater.* **2013**, *1*, 011002.
(41) Saadi, S.; Abild-Pedersen, F.; Helveg, S.; Sehested, J.; Hinnemann, B.; Appel, C. C.; Nørskov, J. K. On the role of metal step-edges in graphene growth. *J. Phys. Chem. C* **2010**, *114*, 11221−11227.
(42) Zheng, J.; Wang, Y.; Wang, L.; Quhe, R.; Ni, Z.; Mei, W.-N.; Gao, Z.; Yu, D.; Shi, J.; Lu, J. Interfacial properties of bilayer and trilayer graphene on metal substrates. *Sci. Rep.* **2013**, *3*, 2081.
(43) Medford, A. J.; Shi, C.; Hoffmann, M. J.; Lausche, A. C.; Fitzgibbon, S. R.; Bligaard, T.; Nørskov, J. K. CatMAP: A software package for descriptor-based microkinetic mapping of catalytic trends. *Catal. Lett.* **2015**, *145*, 794−807.
(44) Bronsted, J. N. Acid and basic catalysis. *Chem. Rev.* **1928**, *5*, 231−338.
(45) Page, A. J.; Ding, F.; Irle, S.; Morokuma, K. Insights into carbon nanotube and graphene formation mechanisms from molecular simulations: A review. *Rep. Prog. Phys.* **2015**, *78*, 036501.
(46) Dai, X.; Mitchell, I.; Kim, S.; An, H.; Ding, F. Multilayer graphene sunk growth on Cu(111) surface. *Carbon* **2022**, *199*, 233−240.
(47) Nørskov, J. K.; Abild-Pedersen, F.; Studt, F.; Bligaard, T. Density functional theory in surface chemistry and catalysis. *Proc. Natl. Acad. Sci. U. S. A.* **2011**, *108*, 937−943.
(48) Li, X.; Chiong, R.; Hu, Z.; Page, A. J. Low-cost Pt alloys for heterogeneous catalysis predicted by density functional theory and active learning. *J. Phys. Chem. Lett.* **2021**, *12*, 7305−7311.
(49) Li, X.; Chiong, R.; Page, A. J. Group and period-based representations for improved machine learning prediction of heterogeneous alloy catalysts. *J. Phys. Chem. Lett.* **2021**, *12*, 5156−5162.
(50) Okamoto, H., Schlesinger, M., Mueller, E., Eds. *Alloy Phase Diagrams*; ASM International, 2016; pp 520−533.
(51) Chakrabarti, D. J.; Laughlin, D. E. The Cu-Y (Copper-Yttrium) system. *Bull. Alloy Phase Diagrams* **1981**, *2*, 315−319.
(52) Waterstrat, R.; Shapiro, A.; Jeremie, A. The palladium−zirconium phase diagram. *J. Alloys Compd.* **1999**, *290*, 63−70.
(53) Pan, S. J.; Yang, Q. A survey on transfer learning. *IEEE Trans. Knowl. Data Eng.* **2010**, *22*, 1345−1359.
(54) Hu, W.; Liu, B.; Gomes, J.; Zitnik, M.; Liang, P.; Pande, V. S.; Leskovec, J. Strategies for pre-training graph neural networks. 8th International Conference on Learning Representations, ICLR, 2020.

https://doi.org/10.1021/acs.nanolett.3c02496
Nano Lett. 2023, 23, 9796−9802